AGU PUBLICATIONS

JGR

Journal of Geophysical Research: Atmospheres

RESEARCH ARTICLE
10.1002/2015JD024115

Key Points:
- Classification of aerosol types including mineral dust, OC, BC, and secondary inorganic ions
- Interpretation of monthly variations of the aerosol types by meteorology and emissions
- Application of the results to well-characterized global AERONET sites to confirm their validity

Correspondence to:
Y. S. Ghim,
ysghim@hufs.ac.kr

Citation:
Choi, Y., Y. S. Ghim, and B. N. Holben (2016), Identification of columnar aerosol types under high aerosol optical depth conditions for a single AERONET site in Korea, *J. Geophys. Res. Atmos.*, *121*, 1264–1277, doi:10.1002/2015JD024115.

Received 22 AUG 2015
Accepted 14 JAN 2016
Accepted article online 16 JAN 2016
Published online 6 FEB 2016

Identification of columnar aerosol types under high aerosol optical depth conditions for a single AERONET site in Korea

Yongjoo Choi[1], Young Sung Ghim[1], and B. N. Holben[2]

[1]Department of Environmental Science, Hankuk University of Foreign Studies, Yongin, Korea, [2]NASA Goddard Space Flight Center, Greenbelt, Maryland, USA

Abstract Dominant aerosol types were classified using level 2 inversion products for the Anmyon Aerosol Robotic Network (AERONET) site in Korea for the period 1999–2007. The aerosol types were mineral dust (MD), MD mixed with carbon, and black carbon mixed coarse particles (BCCP) for coarse mode aerosols, black carbon (BC), organic carbon (OC), and secondary inorganic ions (SII) for fine mode aerosols, and mixed particles between. The classification was carried out using a clustering method based on parameters, including single scattering albedo (SSA), absorption Angstrom exponent (AAE), and fine mode volume fraction (FMVF). Among the seven aerosol types, MD was distinct, with the highest AAE and a very low FMVF and SII with the highest SSA and FMVF. BCCP was introduced to designate coarse particles mixed with BC, of which the AAE was lower than 1, despite a low FMVF. In addition to a large difference in AAE between BC and OC, the SSA of OC was larger than that of BC, indicating the effects of the white smoke produced from the smoldering phase of biomass burning. Monthly variations of the aerosol types were well interpreted by meteorology and emissions and coincided with those in the previous studies. Applying our results to well-characterized global AERONET sites, we confirmed that the aerosol types at Anmyon were valid at other sites. However, the results also showed that the mean properties for aerosol types were influenced by the specific aerosols prevalent at the study sites.

1. Introduction

Although uncertainties in the effects of aerosols on climate change have continued to be relieved over the past few decades, the scientific understanding of aerosols is still much lower compared with that of greenhouse gases such as CO_2 and CH_4 [*Intergovernmental Panel on Climate Change*, 2007, 2013]. Dealing with aerosols incurs major difficulties due to the large spatial and temporal variations resulting from their shorter residence time. These difficulties are further compounded by the maldistribution of information on aerosols, both spatially and temporally, which means that information is not properly provided as occasion demands.

With growing interest in aerosols, ground-based remote sensing measurements from networks such as Aerosol Robotic Network (AERONET) [*Holben et al.*, 2001] and Skyradiometer Network (SKYNET) [*Takamura et al.*, 2004] have become the subject of many studies. Initially, these networks were deployed to compare and validate satellite observations [*Holben et al.*, 2001]. However, as the number of measurement sites increases, many advantages of ground-based measurements have been acknowledged. Ground-based measurements can provide steady information at fixed locations, and their coverage now extends to almost every part of the world with an ever increasing number of sites. Furthermore, remote sensing measurements of column aerosols have merits over in situ physical and chemical measurements of surface aerosols; column data are more useful in estimating the radiative forcing, and remote sensing measurements require less labor and cost than intricate physical and chemical measurements.

One of the promising research subjects using data from ground-based remote sensing measurement networks is the identification of dominant aerosol types at a specific site or region. This type of information has been available only from long-term measurements of speciated aerosol data, which are implemented in selected areas, mostly in the United States and Europe. On the other hand, *Omar et al.* [2005] categorized global atmospheric aerosols using the archive of the AERONET data set from more than 250 sites worldwide. They identified six aerosol types representing desert dust, biomass burning, polluted continental, background/rural, polluted marine, and dirty pollution, using 26 parameters consisting of size distribution and optical properties such as mean radius and single scattering albedo (SSA).

Table 1. Selected Studies for Classification of Dominant Aerosol Types

Date Source	Reference	Parameters[a]	Study Area (Period)	Aerosol Types
AERONET	This study	SSA_{440}, $AAE_{440-1020}$, and FMVF	Anmyon, Korea (1999–2007)	Mineral dust (MD), MD + carbon, BC mixed coarse particles, mixed, OC, BC, and secondary inorganic ions
	Omar et al. [2005]	26 variables[b] of AERONET	Worldwide (>250 sites; up to 2002)	Desert dust, biomass burning, background/rural, polluted continental, polluted marine, and dirty pollution
	Russell et al. [2010]	$AAE_{440/1020}$ and $AE_{440/870}$	Worldwide (11 sites; up to 2000)	Urban-industrial, biomass burning, and desert dust
	Lee et al. [2010]	FMF_{550} and SSA_{440}	Worldwide (not specified)	Dust, mixture, nonabsorbing fine mode, and BC (slightly, moderately, and highly absorbing)
	Giles et al. [2012]	SSA_{440}, $AAE_{440-870}$, $AE_{440-870}$, and FMF_{550}	Worldwide (1999–2010)	Dust, mixed, urban/industrial, and biomass burning
	Cazorla et al. [2013]	$AAE_{440/675}$ and $SAE_{440/675}$	Worldwide (33 sites; not specified)	Dust dominated, dust/EC mix, coated large particles, OC/dust mix, OC dominated, EC/OC mix, EC dominated, and mix
MODIS and OMI	*J. Kim et al.* [2007]	FMF (MODIS) and AI (OMI)	East Asia (ABC-EAREX; 2005)	Dust, carbonaceous, sea salt, and sulfate
AERONET and CALIOP	*Mielonen et al.* [2009]	SSA_{440}, $AE_{440-870}$ (AERONET), depolarization ratio, integrated attenuated backscatter coefficient, surface type, and layer heights (CALIOP)	Worldwide (38 AERONET sites; since June 2006)	Dust, polluted dust, biomass burning, marine, clean continental, and polluted continental
In situ chemical and physical measurements	*Yang et al.* [2009]	$AAE_{470-660}$ and $SAE_{450-700}$	Xianghe, China (2005.3.2–3.26)	Biomass burning, dust, fresh chimney plume, other coal pollution, and background air

[a] $\phi_\lambda = \phi$ at λ nm; $\phi_{\lambda 1 - \lambda 2}$ = slope of the best fit line from the plot of ln ϕ versus ln λ; and $\phi_{\lambda 1/\lambda 2}$ = ln $(\phi_{\lambda 1}/\phi_{\lambda 2})$/ln $(\lambda 1/\lambda 2)$.
[b] Complex refractive index (8), mean radius (2), single scattering albedo (4), standard deviation (2), asymmetry factor (4), mode total volume (2), and extinction/backscatter ratio (4) at four wavelengths (441, 673, 873, and 1022 nm) of AERONET. The number in the parentheses indicates the number of variables.

Table 1 summarizes the previous studies classifying dominant aerosol types. *Russell et al.* [2010] distinguished urban-industrial, biomass burning, and desert dust aerosols using Angstrom exponent (AE) and absorption Angstrom exponent (AAE). Their results were derived from various studies investigating the differences in spectral dependency of absorption between black carbon (BC), organic carbon (OC), and desert dust [*Eck et al.*, 1999; *Bergstrom et al.*, 2004, 2007]. The study by *Russell et al.* [2010] was elaborated by *Giles et al.* [2012] using two further parameters of SSA and the fine mode fraction (FMF) of aerosol optical depth and by introducing the mixtures of absorbing aerosols. Recently, *Cazorla et al.* [2013] divided eight aerosol types on the domain of AAE versus scattering AE, allocating various types of mixed aerosols between three ideal absorbing species, elemental carbon (EC), OC, and mineral dust, based on the study by *Bahadur et al.* [2012].

Lee et al. [2010] classified aerosol types into coarse mode dust, mixture, and nonabsorbing and absorbing fine mode aerosols using FMF and SSA. This approach is important because four aerosol types were divided using two basic parameters and only distinct types were identified by designating intermediate groups into uncertain and mixture groups. Classification of four aerosol types including dust, sea salt, carbonaceous materials, and sulfate by considering fine and coarse modes and absorption and scattering is commonly used in the analysis of satellite data [*Higurashi and Nakajima*, 2002; *J. Kim et al.*, 2007]. *Mielonen et al.* [2009] compared the Cloud-Aerosol Lidar with Orthogonal Polarization (CALIOP) satellite data and AERONET data using SSA and AE and separated six aerosol types by allowing intermediate groups between coarse and fine aerosols and between absorbing and nonabsorbing aerosols.

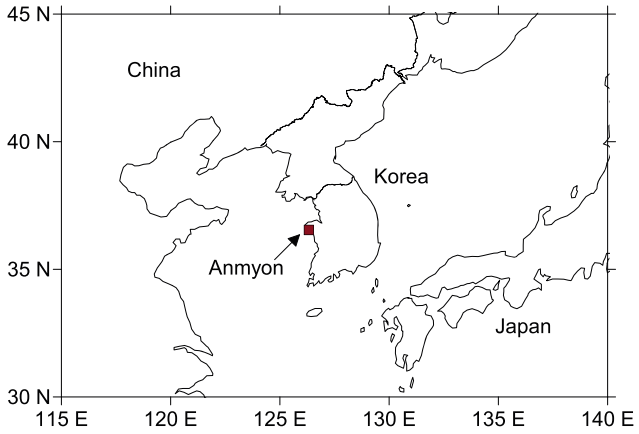

Figure 1. Location of the Anmyon AERONERT site.

Yang et al. [2009] measured scattering and absorption along with chemical and physical properties including OC and EC, as well as size distributions, during the East Asian Study of Tropospheric Aerosols: an International Regional Experiment (EAST-AIRE) campaign. With these intensive measurements, they were able to discriminate detailed variations in the absorption properties of dominant aerosol types in the air masses arriving at a site. *Cazorla et al.* [2013] used in situ optical and chemical measurement data during three aircraft field campaigns performed in California to validate an aerosol classification methodology using spectral optical properties by comparing the results with aerosol sources determined by an aerosol time-of-flight mass spectrometer. While almost 60% of aerosols from secondary biomass burning sources were classified into OC and OC mixed, carbonaceous aerosols from fossil fuel and biomass burning origins were not clearly distinguished. Most dust aerosols were not correctly classified, which was considered to be due to the small number of dust measurements.

The aim of the present study was to identify dominant aerosol types for Anmyon (36.54°N, 126.33°E), an AERONET site located on the west coast of the Korean Peninsula (Figure 1). Although the site is regarded as a typical rural or background site in Korea, without major sources nearby [*S.-W. Kim et al.*, 2007], it is affected by the transport of anthropogenic pollutants from the Asian Continent associated with prevailing westerlies. As a result, *Omar et al.* [2005] classified the Anmyon site as a polluted continental site along with similar amounts of fine and coarse mode aerosols [*Eck et al.*, 2005]. In this study, we distinguished dominant aerosol types for the Anmyon site using the AERONET data archive between 1999 and 2007. We then examined the characteristics of each aerosol type, such as differences in mean properties and the monthly variations of their occurrence rates. Next, we classified aerosols at the AERONET sites that have clearly different source characteristics into the aerosol types identified for the Anmyon site and compared the results to those from previous studies for the same sites to ensure the validity of the present approach.

2. Methods

An automatic tracking sun and sky scanning radiometer, CE 318 (CIMEL Electronique; also called a sunphotometer) is used to measure the direct and diffuse radiation at AERONET sites [*Holben et al.*, 1998]. Direct radiation is measured with a 1.2° full field of view every 15 min at 340, 380, 440, 500, 675, 870, 940, and 1020 nm (nominal wavelengths), and aerosol optical depth (AOD) is retrieved at all wavelengths, except at 940 nm, which is used for retrieving column water vapor [*Holben et al.*, 2001; *Eck et al.*, 2010]. Diffuse radiation is measured on the principal plane (with a fixed azimuth angle and varied zenith angle) and the almucantar plane (with a fixed zenith angle and varied azimuth angle up to 180° on both sides) using four wavelength channels (440, 675, 870, and 1020 nm) [*Holben et al.*, 2001]. Diffuse radiation in the almucantar geometry is measured at the optical air masses of 4, 3, 2, and 1.7 in both morning and afternoon and hourly between [*Eck et al.*, 2010]. Using almucantar measurements, the volume size distribution and complex refractive indices are determined by comparing AOD with that from direct radiation measurements, and other parameters such as SSA are retrieved [*Dubovik et al.*, 2000, 2006].

In this study we used the level 2 inversion product which is cloud screened and quality assured by applying the criteria such as that for solar zenith angle (SZA $\geq$ 50°) [*Smirnov et al.*, 2000; *Holben et al.*, 2006]. As shown in Table 1, we employed three parameters to identify aerosol types. AAE and fine mode volume fraction (FMVF) were selected to separate the absorbing aerosols according to recent studies [*Russell et al.*, 2010; *Giles et al.*, 2012; *Cazorla et al.*, 2013]. SSA was used to further distinguish the scattering aerosols [*Lee et al.*, 2010; *Giles et al.*, 2012]. Note that we used FMVF instead of AE to discern the dominant size because AE does not provide

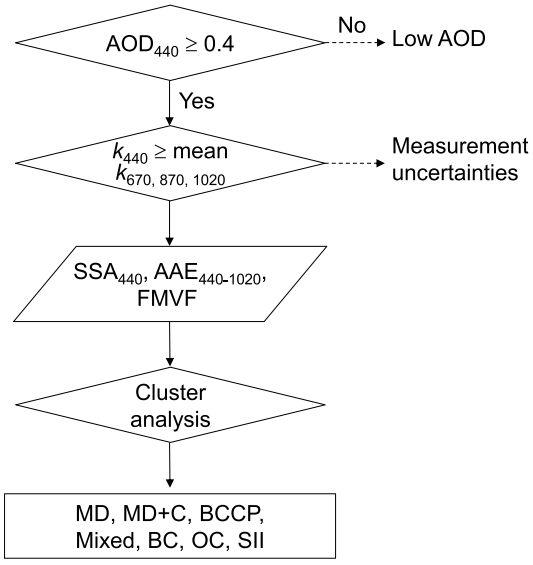

Figure 2. Flowchart for the classification of aerosol types. MD, mineral dust; MD + C, mineral dust mixed with carbon; BCCP, black carbon mixed coarse particles; BC, black carbon; OC, organic carbon; SII, secondary organic ions.

clear information in the intermediate range between 1 and 2, which occurs frequently for atmospheric aerosols [*Schuster et al*., 2006; *Prats et al*., 2011]. FMVF was determined as the fraction of the volume concentration below the local minimum of the bimodal distribution, which was in the range of 0.44–0.99 μm, between fine and coarse modes [*Dubovik et al*., 2002; *Schafer et al*., 2008; *Prats et al*., 2011].

Figure 2 shows the classification method for dominant aerosol types in this study. First, AOD_{440} less than 0.4 was separated as "low AOD" because this AOD is too low to obtain valid optical properties to identify the aerosol type. We examined the portion of aerosols of low AOD in comparison with that of dominant aerosols, considering that AOD ≥ 0.4 was infrequent. Despite recent attempts to utilize the data of AOD < 0.4 to improve the data coverage [*van Beelen et al*., 2014], we decided to adopt a widely used approach excluding low AOD, as in the previous studies shown in Table 1. This was because the primary aim of this study was to obtain relevant information on dominant aerosol types from the AERONET data set at a target site in a common way, which has been available only from long-term intricate in situ measurements.

Next, the imaginary part of the refractive index at 440 nm less than the mean of the indices at 670, 870, and 1020 nm was excluded according to *Arola et al.* [2011]. This was because the imaginary refractive index is constant for BC and decreases with the wavelength for OC and dust [*Kirchstetter et al*., 2004; *Chin et al*., 2009]. Considering the large uncertainty of the imaginary refractive index, 30%–50% [*Dubovik et al*., 2000], we also attempted the classification without this restriction. However, we failed to obtain a plausible result mainly because of the improper allocation of AAE among aerosol types. The total number of level 2 inversion products at Anmyon for the study period was 1537. Two thirds of these (1033) were classified as low AOD (AOD < 0.4). Ten percent (154) were removed because of the restriction of the imaginary refractive index, and 23% (350) were used to determine dominant aerosol types.

The dominant aerosol types were distinguished using an *R* function, hierarchical clustering (https://stat.ethz.ch/R-manual/R-devel/library/stats/html/hclust.html), included in the standard *R* package, "stats" with the option of ward (ward.D in R versions newer than 3.0.3). As mentioned previously, we used SSA, AAE, and FMVF for the cluster analysis. Another R function, linear discriminant analysis (https://cran.r-project.org/web/packages/lda/index.html), which is provided as a function of the "mass" package, was used to classify aerosols at worldwide AERONET sites into the aerosol types obtained from the Anmyon site.

Figure 3 shows the separation of aerosol types with increasing number of clusters. The first two clusters were separated according to the wavelength dependence of absorption into those with higher and lower AAE (mean values of 1.51 and 1.08, respectively). With the increase of the number of clusters to three, aerosols with higher AAE were divided into a cluster with a more higher AAE (2.46) and low FMVF (0.09) designated as MD and a cluster with increased FMVF (0.42) and a large number of data designated as "OC mixed." At five clusters, the OC mixed was further divided into OC and "coarse mode mixed" composed of MD mixed with carbon (MD + C) and mixed particles at six clusters. Aerosols with lower AAE were divided into BC mixed coarse particles (BCCP) characterized by even lower AAE (0.97) than BC and low FMVF (0.30) and "fine mode mixed" composed of BC and secondary inorganic ions (SII) at seven clusters.

At eight clusters, further division of OC resulted in two groups with a similar amount of data, one with higher AAE (1.91) and lower FMVF (0.46) and the other with lower AAE (1.57) and higher FMVF (0.70). The first group could be assumed to be mixed with MD and the second group with BC. However, this division was considered to be relatively insignificant, so seven was chosen as the optimum number of clusters.

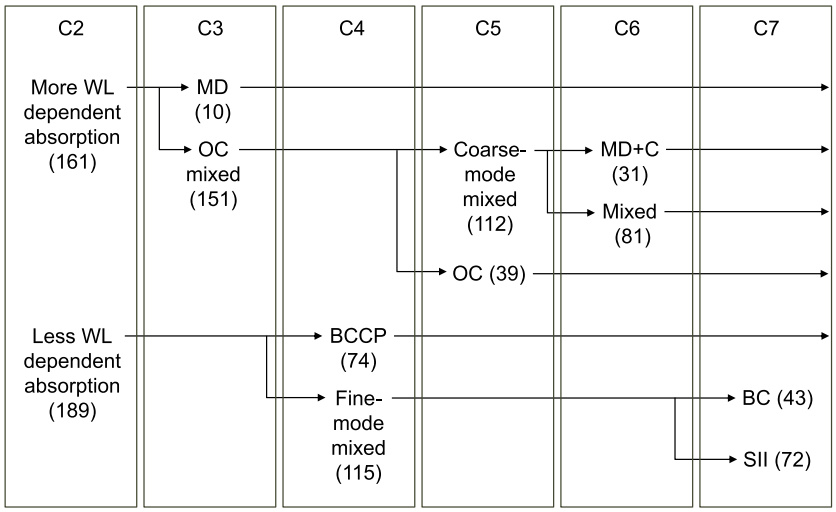

Figure 3. Separation of aerosol types with increasing number of clusters. C2 to C7 denote two to seven clusters, respectively. WL is an abbreviation of wavelength. The numbers in the parentheses denote the number of data.

3. Results and Discussion

3.1. Properties of Dominant Aerosol types

Figure 4 shows the separation of each aerosol type within the domain of two parameters chosen from the three parameters used for the cluster analysis (Figure 2). MD, for example, denotes MD type aerosols, but MD is used throughout the present study for simplicity. Although the number of aerosol types is not small,

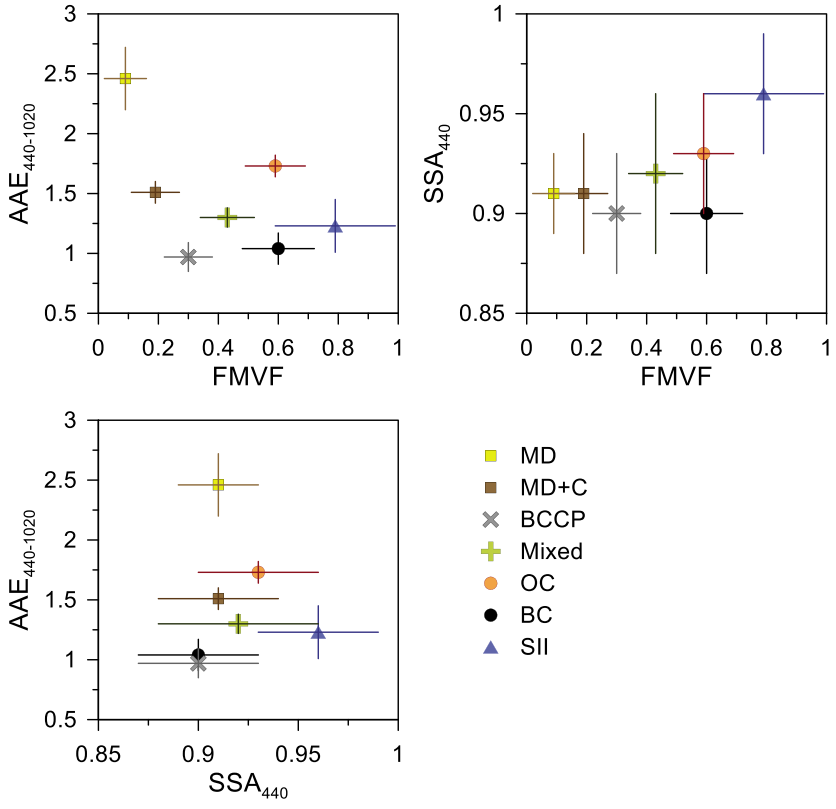

Figure 4. Separation of dominant aerosol types on the domain of two parameters chosen from three parameters used for the cluster analysis. Error bars denote the standard deviation.

Table 2. Mean Properties of Dominant Aerosol Types (Mean ± Standard Deviation) and Their Fractions of Occurrences at Anmyon for the Period 1999–2007

Aerosol Type	SSA_{440}	$AAE_{440-1020}$	FMVF	$AE_{870/440}$	AOD_{440}	Fraction
MD	0.91 ± 0.02	2.46 ± 0.26	0.09 ± 0.07	0.23 ± 0.19	1.07 ± 0.72	2.9%
MD + C	0.91 ± 0.03	1.51 ± 0.09	0.19 ± 0.08	0.64 ± 0.19	0.72 ± 0.31	20.6%
BCCP	0.90 ± 0.03	0.97 ± 0.12	0.30 ± 0.08	0.97 ± 0.29	0.63 ± 0.34	8.86%
Mixed	0.92 ± 0.04	1.30 ± 0.08	0.43 ± 0.09	1.15 ± 0.13	0.64 ± 0.17	12.6%
OC	0.93 ± 0.03	1.73 ± 0.09	0.59 ± 0.10	1.17 ± 0.21	0.76 ± 0.22	22.9%
BC	0.90 ± 0.03	1.04 ± 0.13	0.60 ± 0.12	1.22 ± 0.30	0.63 ± 0.23	21.1%
SII	0.96 ± 0.03	1.23 ± 0.22	0.79 ± 0.20	1.40 ± 0.23	0.70 ± 0.30	11.1%

the separation is relatively good, except for BC and BCCP on the domain of AAE versus SSA. However, these two types are also easily separable in the other two domains. Smaller deviations indicate that AAE is a good parameter for distinguishing aerosol types compared with FMVF and SSA, even including SII with minimal absorption. Among the seven aerosol types, the most ambiguous is mixed particles. The FMVF of mixed particles is between MD, MD + C, and BCCP in the coarse mode and OC, BC, and SII in the fine mode. AAE is between MD, OC, and MD + C, which show enhanced absorption at short wavelengths, and SII, BC, and BCCP of which absorption enhancement at short wavelengths is not pronounced. SSA is higher than BC/BCCP and MD/MD + C but lower than SII and OC.

Table 2 shows the mean properties of the dominant aerosol types distinguished in this study. As shown in Figure 4, MD is characterized by high AAE and low FMVF. The FMVF of 0.09 is particularly low, which could be considered as pure dust with a minimum contribution of fine mode aerosols [*Kim et al*., 2011]. Because MD is confined to pure dust, AAE shown in Table 2 is in the upper part of the generally reported range of AAE for MD between 1.0 and 3.0 [*Russell et al*., 2010, 2014; *Giles et al*., 2012; *Cazorla et al*., 2013]. On the other hand, SSA is close to that of BC or BCCP and MD + C, which approaches the lower limit of the generally reported range of SSA for MD between 0.90 and 0.95 [*Giles et al*., 2012; *Russell et al*., 2014]. Recently, *Khatri et al.* [2014] demonstrated that SSA of dust could be lowered due to the increase of the coarse fraction without changes in the chemical composition. Therefore, low SSA of MD in this study is also attributable to low FMVF to some extent.

In addition to the three parameters used for the cluster analysis, AE is provided in Table 2 because many studies reported their results using AE rather than FMVF. Table 2 also shows AOD along with the fraction of each aerosol type. Although the AOD of MD is the highest among the seven aerosol types, this level of AOD (1.07 ± 0.72) is not high enough compared with that in other studies such as *Cachorro et al.* [2008] and *Wu et al.* [2009], which reported peak values of 2.7 and 2.52, respectively. Considering that their lowest values were 0.5 or lower, the AOD of MD shown in Table 2 could be reasonable as a mean value. The fraction of MD is only 2.9% as a large part of MDs is mixed with carbon. Because carbon predominantly occurs as fine particles, the FMVF of MD + C increases to 0.19, even if it is still low. SSA is basically not altered, but AAE is lowered by mixing with carbon. *Yang et al.* [2009] indicated that the AAE of dust in Beijing measured using an aethalometer decreased to 1.82 ± 0.90 since dust aerosols were mixed with BC. The AAE of dust measured using an aethalometer at Gosan was reported to be even lower at 1.2–1.8, due to the inclusion of pollutants [*Lee et al*., 2012].

The SSA of BCCP is as low as that of BC, but the FMVF is higher than those of MD and MD + C. Furthermore, the mean value of AAE is lower than BC and below 1.0. Many studies dealing with carbonaceous aerosols considered the AAE of BC of around 0.8 and 1.1 as a lower limit [*Bergstrom et al*., 2002; *Kirchstetter et al*., 2004; *Bahadur et al*., 2012]. However, *Gyawali et al.* [2009] found from both measurement and simulation that the AAE of aged BC coated with nonabsorbing materials could decrease below 1.0. If BC was coated with absorbing (organic) materials, AAE was generally higher than 1.0 or more due to the spectral dependency of organic materials but also reduced to below 1.0 when the absorption by the coating material decreased with the decreasing imaginary refractive index [*Lack and Cappa*, 2010].

According to *Cazorla et al.* [2013], the AAE and FMVF of BCCP in Table 2 correspond to those between dust/EC mix and coated large particles. However, we believe that AAE could not be reduced to below 1.0 by mixing of BC with dust having a high AAE. For the coated large particles, it was uncertain that the coating around the BC core was a prerequisite to such a low AAE, although reducing AAE has been demonstrated, assuming

concentric core-and-shell particles. This was because studies based on other types of particle mixing did not seem to be sufficient [*Bond and Bergstrom*, 2006]. Furthermore, studies focusing on coated BC particles did not show that coated BC particles could grow to large or coarse particles [*Gyawali et al*., 2009; *Lack and Cappa*, 2010; *Liu et al*., 2014; *Taylor et al*., 2014]. We finally decided to use the term BCCP to refer to BC mixed coarse particles, selecting BC as a key to low AAE and selecting coarse particles to explain low FMVF. We did not clarify the way BC was mixed into coarse particles, as this was considered a subject of future studies.

As seen in Figure 4, the mixed particles are an aerosol type, which is not clearly defined between fine and coarse modes (the sums of fractions are 55% and 32%, respectively) and between high and low spectral dependences of absorption (46% and 41%, respectively). Although the SSA of the mixed particles is higher than strong absorbing aerosols such as BC, MD, and their mixtures (53%), the mixed particles could be classified as an absorbing aerosol because the SSA of the mixed particles is still lower than that of OC, of which the absorbing property has been a crucial issue during the past decade [*Kirchstetter et al*., 2004; *Pöschl*, 2005; *Andreae and Gelencsér*, 2006; *Russell et al*., 2010].

The difference in AAE between BC and OC has been noted in many studies [e.g., *Cazorla et al*., 2013], but the SSAs of BC and OC are not much different in Table 2 and Figure 4 due to a comparatively high SSA of OC. Carbonaceous aerosols from biomass burning have a large variation depending on the combustion conditions (flaming versus smoldering). Flaming produces dark smoke with lower SSAs, while smoldering produces white smoke with higher SSAs [*Russell et al*., 2014]. Although the difference in darkness of the smoke is understood to correlate with the level of BC contents [*Eck et al*., 2013], it is also attributable to the variations in OC, considering a continuous spectrum of chemical and optical properties of OC depending on the fraction of carbon [*Pöschl*, 2005; *Andreae and Gelencsér*, 2006]. In fact, the SSA of OC in Table 2 coincides well with the higher SSA of biomass burning aerosols between 0.92 and 0.94 [*Giles et al*., 2012; *Russell et al*., 2014].

FMVFs of BC and OC are similarly around 60%. Because OC and BC mostly exist in fine particles in areas influenced by anthropogenic emissions [*Kim et al*., 2000; *Putaud et al*., 2004; *Minoura et al*., 2006], a higher FMVF was expected, particularly for BC. Not only 60% of FMVF is lower than 70%–80% of urban/industrial and biomass burning aerosols as reported in *Russell et al.* [2014] but also the corresponding AE of 1.2 is lower than 1.5–2.0 of the same aerosols reported in *Russell et al.* [2010] and *Giles et al.* [2012]. Taking into account the vast effect of MD or fugitive dust in the Korean Peninsula as well as in other areas in Northeast Asia [*Kim et al*., 2008; *Choi et al*., 2014], the effect of MD may not have been clearly discerned, despite the separation of MD + C.

The mean properties of SII are most distinct on the domain of SSA versus FMVF with the highest SSA and FMVF, similarly to those of MD on the domain of AAE versus FMVF, as shown in Figure 4. The highest SSA is easily anticipated because only the SII is a scattering aerosol in Table 2. Nevertheless, it is true that the SSA of SII in Table 2 is not high, considering the minimal values of the imaginary refractive indices of the SII [*Seinfeld and Pandis*, 1998]. However, in the Tropical Aerosol Radiative Forcing Observational Experiment (TARFOX), where concentrations of non-sea-salt sulfate and ammonium were higher than in other campaigns [*Quinn and Bates*, 2005], SSA varied from 0.90–0.98 depending on the measurement instrument, relative humidity, and altitude [*Russell et al*., 2002]. *Levy et al.* [2007] and *Lee et al.* [2010] used the value of 0.95 as a criterion to separate scattering aerosols from absorbing aerosols. The SSA of SII is reduced due to the inclusion of absorbing aerosols in the real atmosphere, and the slightly higher AAE than 1.0 can be understood in the same context.

It is important to note that only SII is distinguished as a scattering aerosol in Table 2 without sea salt, although Anmyon is located on the coast. This is because AOD in pure maritime environments dominated by sea salt is typically less than 0.1 [*Smirnov et al*., 2002, 2011], which is significantly below 0.4, the limit for the AERONET level 2 inversion product.

3.2. Monthly Variations in Dominant Aerosol Types

Figure 5 shows the monthly variation in the occurrence rate of dominant aerosol types along with aerosols of low AOD (AOD < 0.4). The occurrence rate was calculated by dividing the occurrence number of the aerosol type by the total number of almucantar raw data for SZA between 50° and 80° from which inversion products were obtained [*García et al*., 2008]. This means that the occurrence rate represents the number of times dominant aerosol types occur during the valid operating hours of the instrument when the instrument measures diffuse radiation in the almucantar geometry that can be used for inversion products.

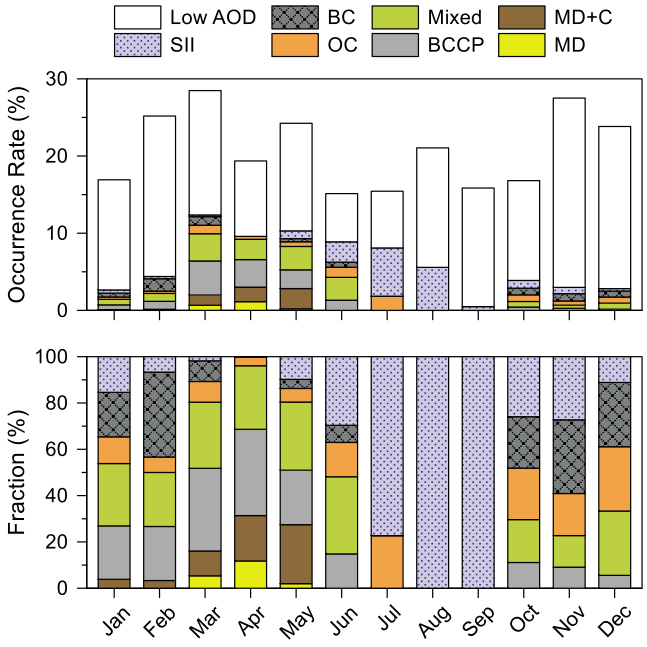

Figure 5. Monthly variations in the occurrence rates of dominant aerosol types along with aerosols of low AOD and the fractions of dominant aerosol types at Anmyon for the period 1999–2007. Low AOD denotes aerosols with AOD < 0.4.

In Figure 5, the monthly total of the occurrence rates including low AOD aerosols varies from 28% in March and November to 15% in June and July. It is important to note that the level of occurrence rate is low, particularly for dominant aerosol types. On an annual basis, the total occurrence rate was 21%, which is the sum of 5.4% for dominant aerosol types and 16% for low AOD aerosols. The annual mean occurrence rate of 5.4% for dominant aerosol types is low enough but could be plausible because high AOD conditions of AOD ≥ 0.4 are uncommon and the level 2 inversion products which are cloud screened and quality assured are rare even in comparison with the valid operating hours (of the instrument).

The number of valid operating hours is high in the colder months between October and February and low in the summer months between June and August. The latter was due to the high percentage of cloud cover during the rainy season (generally late June to mid-July) and the low SZA at midday around the summer solstice (note that level 2 product is available when SZA $\geq 50°$). Monthly variation in the number of level 2 inversion products was similar to that of the valid operating hours. However, the variations in the occurrence rate shown in Figure 5 differ because the occurrence rate is the number of inversion products divided by the number of valid operating hours.

The sum of the occurrence rates of dominant aerosol types (the sum excluding low AOD aerosols) is higher between March and May, which is mainly due to a large amount of MD + C, BCCP, and mixed particles (~80%). The fraction of MD is the highest in this period especially in April [*Sun et al.*, 2001; *Kim*, 2008; *Kim et al.*, 2008], and FMVF is the lowest as shown in Figure 6. The prevalence of coarse particles during this period is due to higher wind speeds and dry conditions (Figure 6), which are favorable for the generation of fugitive dust, along with the inflow of Asian dust [*Choi et al.*, 2014]. The fraction of MD + C is also the highest since MD is generally mixed with carbon as observed by satellite [*Higurashi and Nakajima*, 2002; *J. Kim et al.*, 2007] and in situ measurements [*Bates et al.*, 2004; *S.-W. Kim et al.*, 2005, 2007; *Yang et al.*, 2009; *Jung et al.*, 2010; *Lee et al.*, 2012]. The high amount of BCCP is similarly understood in this context.

The sum of occurrence rates of dominant aerosol types is still high during the summer between July and August, but this is primarily because of a large amount of SII. The fraction of SII increases from May and reaches 100% in August, but the occurrence rate of SII is the highest in July. The high occurrence rate of SII in summer is caused by the active photochemical production associated with high temperatures and large hygroscopic growth at high relative humidity [*Eck et al.*, 2005, 2010; *Pathak et al.*, 2009] (Figure 6). Because the FMVF of SII is the highest among dominant aerosols (Table 2), FMVF is also high in July and August. However, FMVF is higher in July when SII is mixed with OC than in August when the fraction of SII is 100%. Note that the occurrence rate of low AOD aerosols is higher in August than in July. It is presumed that FMVF in August may decrease due to the mingling of sea salt in low AOD aerosols, considering that Anmyon is located on the coast.

The occurrence rates and fractions of BC and OC increase from October when fossil fuel combustion for heating increases and remain high until February. Although the variation in BC is closely related and inversely proportional to air temperature, BC is also emitted from various combustion sources including vehicles, of which the effects are consistent year round [*Bond et al.*, 2004; *Wang et al.*, 2012]. However, BC is not observed

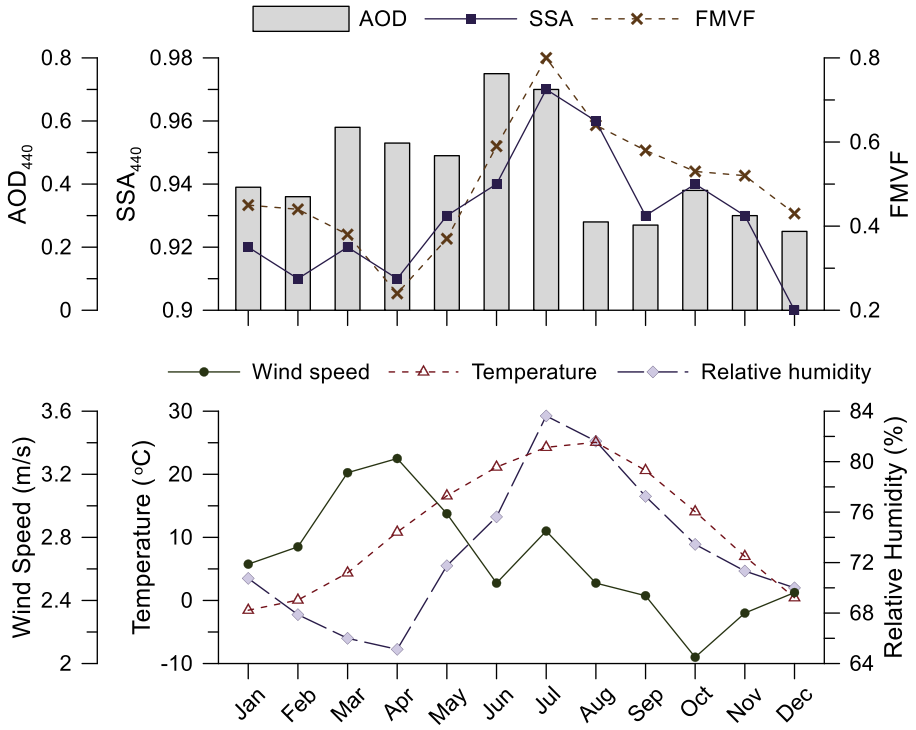

Figure 6. Monthly variations in selected optical, micropysical, and meteorological parameters at Anmyon for the period 1999–2007.

as a dominant aerosol in April and from July to September, probably because the site is located in a rural area where the effects of primary combustion sources are not direct. Situations are similar for OC. However, the occurrence rate and fraction of OC are significant even in June and July, with high temperatures due to the effects of sources that are more diversified such as biomass burning producing OC and secondary formation at high temperatures [*Lim and Turpin*, 2002; *Duan et al*., 2004; *Lim et al*., 2012].

3.3. Dominant Aerosol Types at Selected AERONET Sites

In this section, we classified aerosols at well-characterized worldwide AERONET sites into the dominant aerosol types identified for the Anmyon site (Table 2). The AERONET sites selected are known to have characteristics of urban/industrial (Beijing, China; Mexico City, Mexico; and Goddard Space Flight Center (GSFC), suburban Washington, DC, USA), biomass burning (Mongu, Zambia, and Alta Floresta, Brazil), and dust (Cape Verde, central Atlantic Ocean) [*Dubovik et al*., 2002; *Omar et al*., 2005; *Arola et al*., 2011; *Giles et al*., 2012; *Eck et al*., 2013; *Russell et al*., 2014]. We primarily analyzed the dominant aerosol types at Beijing, Mexico City, and GSFC by comparing with those at Mongu and Alta Floresta as typical types of fine mode aerosols from biomass burning and those at Cape Verde as typical types of coarse mode aerosols from desert dust.

Figure 7 shows the occurrences of aerosol types at the study sites. The study periods vary according to the site because we used all the available data from each site. Beijing is a megacity with heavy aerosol loading generated from various types of fossil fuel combustion, as well as from deserts in the surrounding areas [*Yu et al*., 2009; *Wang et al*., 2011]. Heavy aerosol loading at Beijing is confirmed by the high occurrence rate of dominant aerosol types of about 15%, which is the highest among the sites, and about three times that at Anmyon. The occurrence rates of dominant aerosol types at Mongu and Cape Verde are the next highest but are only one third of that at Beijing. Although the highest occurrence rate at Beijing is primarily due to the coarse mode, the occurrence rate of the fine mode is also the highest [*Eck et al*., 2005, 2010]. The major constituents of the dominant aerosol types at Beijing are BC, OC, and MD + C, in addition to mixed particles and BCCP which are not well characterized. At Beijing, the sum of the occurrence rates of MD and MD + C is 2.1%, compared to 4.2% at Cape Verde, and the sum of the occurrence rates of BC and OC is 4.8%, the highest among the sites.

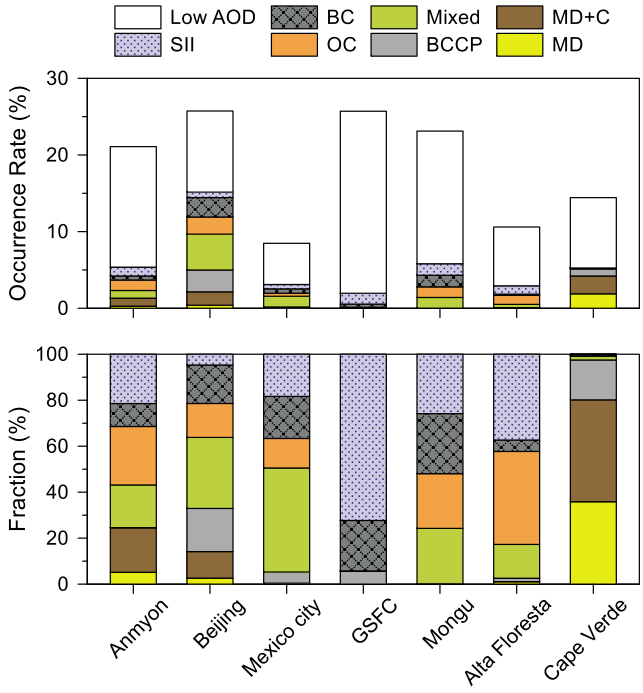

Figure 7. (a) Occurrence rates of dominant aerosol types along with aerosols of low AOD and (b) fractions of dominant aerosol types at selected AERONET sites in comparison with those of the Anmyon site. Study periods: Anmyon (1999–2007), Beijing (2001–2011), Mexico City (1999–2010), GSFC (1993–2011), Mongu (1995–2009), Alta Floresta (1993–2010), and Cape Verde (1993–2010).

Figure 8 shows the mean properties of major categories of dominant aerosol types according to the site. AODs at Beijing are among the highest for all categories, denoting high aerosol loading regardless of aerosol types. Only for BC + OC, the AOD at Alta Floresta mainly affected by biomass burning is higher than that at Beijing. It is worth noting that the AOD for SII is higher than that for the other categories. This means that AOD is generally higher when SII is dominant than when other categories are dominant, although their occurrence rate is low (Figure 7). *Eck et al.* [2005] explained that a high AOD is due to hygroscopic growth in the column associated with high relative humidity in summer. They also mentioned that this high AOD is manifested by high-pressure systems in summer, leading to clear skies that are suitable for sun photometer measurements. On the other hand, generally lower SSAs for dominant aerosol types at Beijing compared to other sites can be attributed to the prevalence of carbonaceous materials [*Eck et al.*, 2010; *Lee et al.*, 2010]. This is particularly true for coarse particles, indicating that the large fraction of coarse particles was mixed with carbon.

Mexico City is another megacity which is known for the severity of air pollution [*World Health Organization/United Nations Environment Programme*, 1992]. However, Figure 7 shows that the occurrence rate of dominant aerosol types at Mexico City is much less than that in Beijing and more similar to Anmyon. A distinct feature of dominant aerosol types at Mexico City in comparison with Beijing and Anmyon is the minimal occurrences of MD and MD + C and the large fraction of mixed particles. This result differs from the findings of other studies [*Querol et al.*, 2008; *Karydis et al.*, 2011], asserting the importance of mineral dust on the level of particulate matter in the Mexico City area. This might be because mineral dust at Mexico City is fugitive and is locally generated in an isolated high-altitude basin, while mineral dust at Beijing and Anmyon originates from distant desert regions that are devoid of major pollution sources. As a result, it is probable that dust over Mexico City is classified as mixed particles with pollutants, including some BCCP, rather than typical mineral dust. Figure 8 shows that AODs at Mexico City are much lower than those at Beijing for all categories and among the lowest for coarse particles and SII. This clearly shows that aerosol loading at Mexico City is low compared with Beijing and other study sites. Generally, lower SSA and higher FMVF for all categories indicates that dominant aerosol types are affected by fine mode carbonaceous aerosols.

GSFC is distinguished from other sites by a high occurrence rate of SII (Figure 7) [*Dubovik et al.*, 2002; *Eck et al.*, 2005]. Among the dominant aerosol types, SII (72%) and BC (22%) account for the most, and BCCP and the minimum amount of the mixed particles account for the remainder. As a result, both the occurrence rate and fraction of coarse particles are the lowest among the study sites [*Dubovik et al.*, 2002]. Mean properties of dominant aerosol types are characterized by lower AOD and AAE but higher SSA and FMVF (Figure 8). The lower AOD is probably due to the effects of SII of which the AOD is generally lower than that of MDs and BC + OC (Table 2). Other characteristics such as lower AAE and higher SSA and FMVF can be similarly interpreted.

Among the remaining three sites, both Mongu and Alta Floresta are primarily influenced by biomass burning (Figure 7). The occurrence rate of dominant aerosol types at Mongu is higher than that at Alta Floresta.

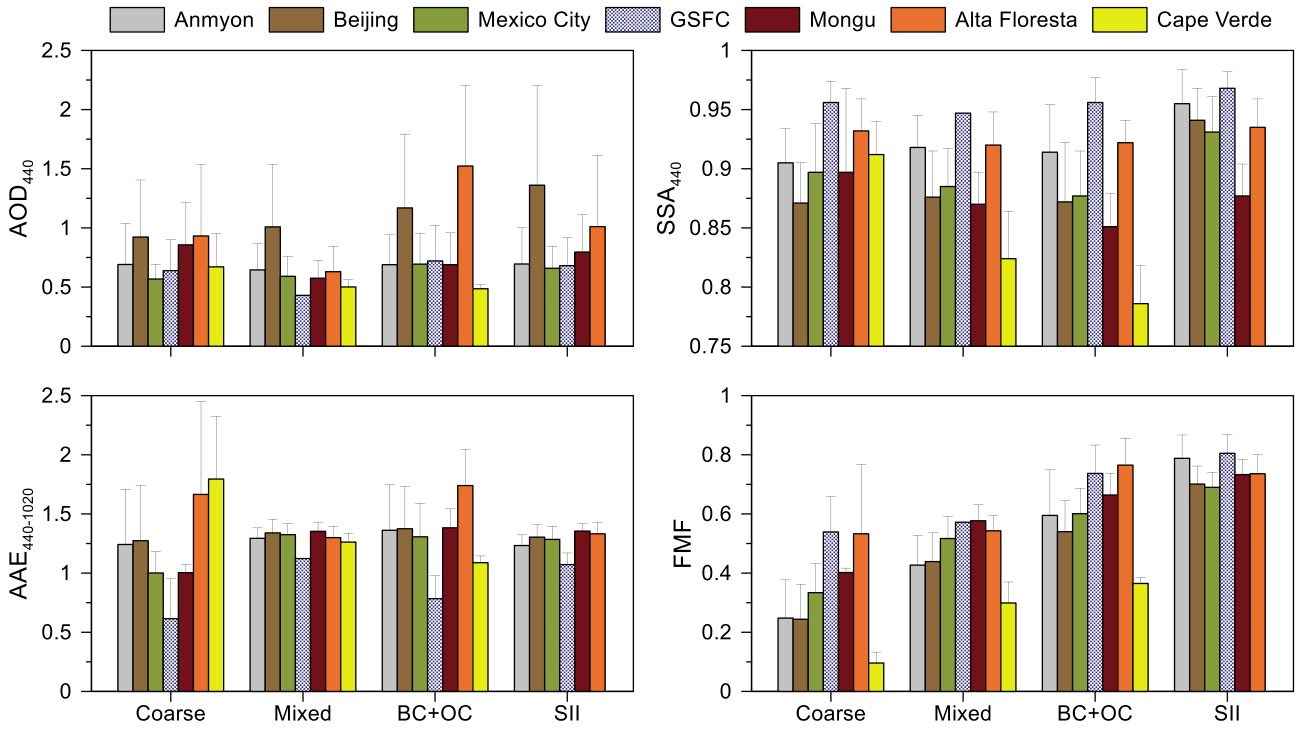

Figure 8. Mean properties of major categories of dominant aerosol types by selected AERONET site. Error bars above bar graphs denote the standard deviation. The term "coarse" represents coarse particles comprising MD, MD + C, and BCCP.

The occurrence rates and fractions of BC and OC are similar at Mongu, while those of OC are much higher than those of BC at Alta Floresta. This is because flaming producing similar amounts of BC and OC at higher temperatures is prevalent at Mongu, while smoldering producing primarily OC at lower temperatures is common at Alta Floresta [*Reid et al.*, 2005; *Arola et al.*, 2011]. The occurrence rate and fraction of SII are comparable to those of BC and OC, indicating photochemical formation of SII due to emissions from biomass burning [*Levine et al.*, 1995]. Although both sites are influenced by biomass burning, the mean properties of aerosol categories differ (Figure 8). The AODs at Alta Floresta are higher than those at Mongu, despite a higher occurrence rate of dominant aerosol types at Mongu because the AOD of OC is higher than that of BC in this study (Table 2). The SSAs at Alta Floresta are higher than those at Mongu for BC + OC because of the higher SSA for OC as well as lower SSA for BC (Table 2). However, SSAs at Alta Floresta are also higher for categories other than BC + OC.

At Cape Verde, the fraction of coarse particles, comprising MD, MD + C, and BCCP, approaches 100% (Figure 7). Although the occurrence rate for coarse particles is also the highest, their mean AOD is in the middle (Figure 8). The lowest FMVF and the highest AAE for coarse particles can be understood by a large contribution of MD. Some studies indicate that Cape Verde was influenced by biomass burning emissions from the Sahel in winter [*Tesche et al.*, 2009; *Kim et al.*, 2011]. It is presumed that coarse particles mixed with BC from biomass burning result in a comparatively large occurrence rate and fraction of BCCP (Figure 7).

4. Summary and Conclusions

The dominant aerosol types at Anmyon, Korea, were identified using the AERONET data archive for the period 1999–2007. While Anmyon is considered to be a rural or background site in Korea, it has been classified as a polluted continental site due to the effects of the transport of pollutants from the Asian Continent [*Eck et al.*, 2005; *Omar et al.*, 2005]. The dominant aerosol types, MD, MD + C, and BCCP for coarse mode aerosols, BC, OC, and SII for fine mode aerosols, as well as the mixed particles between, were distinguished using a hierarchical clustering method with SSA, AAE, and FMVF.

MD has a much higher AOD and AAE and very low FMVF. However, the fraction of MD among dominant aerosol types is less than 3%, and most MD at Anmyon is mixed with carbon (MD + C). BCCP is newly introduced to designate coarse particles mixed with BC, of which the AAE is lower than 1, despite a low FMVF. The fraction

of coarse mode aerosols including MD, MD + C, and BCCP is higher between March and May when meteorological conditions, such as higher wind speeds and dry conditions, are favorable for the generation of fugitive dust, along with inflow of Asian dust. BC and OC differ in AAE because of the AAE of BC, which is close to 1, and is only higher than that of BCCP. However, they also differ in SSA because of the higher SSA of OC, indicating the effects of white smoke produced from the smoldering phase of biomass burning. Although the occurrence rate and fraction of BC are primarily high during the cold season between October and February, those of OC are also significant even in June and July, with high temperatures probably because of biomass burning and secondary formation. SII is most frequent in July and August due to the active photochemical production associated with high temperatures and large hygroscopic growth at high relative humidity. Their properties are distinct among dominant aerosol types with the highest SSA and FMVF.

The occurrences and properties of dominant aerosol types at seven global AERONET sites with distinct aerosol characteristics were examined by allocating aerosols into the same aerosol types identified at Anmyon. Among the urban/industrial sites, Beijing is characterized by major effects of coarse particles, but the effects of fine particles, including carbonaceous aerosols and SII, are also substantial. As a result, the occurrence rate of dominant aerosol types of AOD $>$ 0.4 is the highest among the sites. Analyzing the occurrences and properties of aerosol types at the global sites, we confirmed that the dominant aerosol types at Anmyon are generally valid at other sites. However, the results show that the mean properties for aerosol types are influenced by specific aerosols prevalent at the sites, such as carbonaceous aerosols at Beijing (lowering SSA), fine mode carbonaceous aerosols at Mexico City (lowering SSA and increasing FMVF), and SII at GSFC (lowering AAE and increasing SSA and FMVF).

Acknowledgments

This work was funded by the Korea Meteorological Administration Research and Development Program under the grant KMIPA 2015-6010. We are grateful to the following principal investigators for establishing and maintaining AERONET sites: H.-B. Chen and P. Goloub of Beijing, D. Tanré of Cape Verde, and A. L. Contreras of Mexico City. The data used in this study are available at http://aeronet.gsfc.nasa.gov/cgi-bin/webtool_opera_v2_inv.

References

Andreae, M. O., and A. Gelencsér (2006), Black carbon or brown carbon? The nature of light-absorbing carbonaceous aerosols, *Atmos. Chem. Phys.*, *6*(10), 3131–3148.

Arola, A., G. Schuster, G. Myhre, S. Kazadzis, S. Dey, and S. N. Tripathi (2011), Inferring absorbing organic carbon content from AERONET data, *Atmos. Chem. Phys.*, *11*, 215–225.

Bahadur, R., P. S. Praveen, Y. Xu, and V. Ramanathan (2012), Solar absorption by elemental and brown carbon determined from spectral observations, *Proc. Natl. Acad. Sci. U.S.A.*, *109*, 17,366–17,371.

Bates, T. S., et al. (2004), Marine boundary layer dust and pollutant transport associated with the passage of a frontal system over eastern Asia, *J. Geophys. Res.*, *109*, D19S19, doi:10.1029/2003JD004094.

Bergstrom, R. W., P. B. Russell, and P. Hignett (2002), Wavelength dependence of the absorption of black carbon particles: Predictions and results from the TARFOX experiment and implications for the aerosol single scattering albedo, *J. Atmos. Sci.*, *59*, 567–577, doi:10.1175/1520-0469(2002)059<0567:wdotao>2.0.co;2.

Bergstrom, R. W., P. Pilewskie, J. Pommier, M. Rabbette, P. B. Russell, B. Schmid, J. Redemann, A. Higurashi, T. Nakajima, and P. K. Quinn (2004), Spectral absorption of solar radiation by aerosols during ACE-Asia, *J. Geophys. Res.*, *109*, D19S15, doi:10.1029/2003JD004467.

Bergstrom, R. W., P. Pilewskie, P. B. Russell, J. Redemann, T. C. Bond, P. K. Quinn, and B. Sierau (2007), Spectral absorption properties of atmospheric aerosols, *Atmos. Chem. Phys.*, *7*, 5937–5943.

Bond, T. C., and R. W. Bergstrom (2006), Light absorption by carbonaceous particles: An investigative review, *Aerosol Sci. Technol.*, *40*, 27–67, doi:10.1080/02786820500421521.

Bond, T. C., D. G. Streets, K. F. Yarber, S. M. Nelson, J.-H. Woo, and Z. Klimont (2004), A technology-based global inventory of black and organic carbon emissions from combustion, *J. Geophys. Res.*, *109*, D14203, doi:10.1029/2003JD003697.

Cachorro, V. E., C. Toledano, N. Prats, M. Sorribas, S. Mogo, A. Berjón, B. Torres, R. Rodrigo, J. de la Rosa, and A. M. De Frutos (2008), The strongest desert dust intrusion mixed with smoke over the Iberian Peninsula registered with Sun photometry, *J. Geophys. Res.*, *113*, D14S04, doi:10.1029/2007JD009582.

Cazorla, A., R. Bahadur, K. J. Suski, J. F. Cahill, D. Chand, B. Schmid, V. Ramanathan, and K. A. Prather (2013), Relating aerosol absorption due to soot, organic carbon, and dust to emission sources determined from in-situ chemical measurements, *Atmos. Chem. Phys.*, *13*, 9337–9350, doi:10.5194/acp-13-9337-2013.

Chin, M., T. Diehl, O. Dubovik, T. F. Eck, B. N. Holben, A. Sinyuk, and D. G. Streets (2009), Light absorption by pollution, dust, and biomass burning aerosols: A global model study and evaluation with AERONET measurements, *Ann. Geophys.*, *27*, 3439–3464.

Choi, S.-H., Y. S. Ghim, Y.-S. Chang, and K. Jung (2014), Behavior of particulate matter during high concentration episodes in Seoul, *Environ. Sci. Pollut. Res.*, doi:10.1007/s11356-014-2555-y.

Duan, F., X. Liu, T. Yu, and H. Cachier (2004), Identification and estimate of biomass burning contribution to the urban aerosol organic carbon concentrations in Beijing, *Atmos. Environ.*, *38*, 1275–1282.

Dubovik, O., A. Smirnov, B. N. Holben, M. D. King, Y. J. Kaufman, T. F. Eck, and I. Slutsker (2000), Accuracy assessments of aerosol optical properties retrieved from Aerosol Robotic Network (AERONET) Sun and sky radiance measurements, *J. Geophys. Res.*, *105*, 9791–9806, doi:10.1029/2000JD900040.

Dubovik, O., B. Holben, T. F. Eck, A. Smirnov, Y. J. Kaufman, M. D. King, D. Tanré, and I. Slutsker (2002), Variability of absorption and optical properties of key aerosol types observed in worldwide locations, *J. Atmos. Sci.*, *59*, 590–608.

Dubovik, O., et al. (2006), Application of spheroid models to account for aerosol particle nonsphericity in remote sensing of desert dust, *J. Geophys. Res.*, *111*, D11208, doi:10.1029/2005JD006619.

Eck, T. F., B. N. Holben, J. S. Reid, O. Dubovik, A. Smirnov, N. T. O'Neill, I. Slutsker, and S. Kinne (1999), Wavelength dependence of the optical depth of biomass burning, urban, and desert dust aerosols, *J. Geophys. Res.*, *104*, 31,333–31,349, doi:10.1029/1999JD900923.

Eck, T. F., et al. (2005), Columnar aerosol optical properties at AERONET sites in central eastern Asia and aerosol transport to the tropical mid-Pacific, *J. Geophys. Res.*, *110*, D06202, doi:10.1029/2004JD005274.
Eck, T. F., et al. (2010), Climatological aspects of the optical properties of fine/coarse mode aerosol mixtures, *J. Geophys. Res.*, *115*, D19205, doi:10.1029/2010JD014002.
Eck, T. F., et al. (2013), A seasonal trend of single scattering albedo in southern African biomass-burning particles: Implications for satellite products and estimates of emissions for the world's largest biomass-burning source, *J. Geophys. Res. Atmos.*, *118*, 6414–6432, doi:10.1002/jgrd.50500.
García, O. E., et al. (2008), Validation of AERONET estimates of atmospheric solar fluxes and aerosol radiative forcing by ground-based broadband measurements, *J. Geophys. Res.*, *113*, D21207, doi:10.1029/2008JD010211.
Giles, D. M., B. N. Holben, T. F. Eck, A. Sinyuk, A. Smirnov, I. Slutsker, R. R. Dickerson, A. M. Thompson, and J. S. Schafer (2012), An analysis of AERONET aerosol absorption properties and classifications representative of aerosol source regions, *J. Geophys. Res.*, *117*, D17203, doi:10.1029/2012JD018127.
Gyawali, M., W. P. Arnott, K. Lewis, and H. Moosmüller (2009), In situ aerosol optics in Reno, NV, USA during and after the summer 2008 California wildfires and the influence of absorbing and non-absorbing organic coatings on spectral light absorption, *Atmos. Chem. Phys.*, *9*, 8007–8015, doi:10.5194/acp-9-8007-2009.
Higurashi, A., and T. Nakajima (2002), Detection of aerosol types over the East China Sea near Japan from four-channel satellite data, *Geophys. Res. Lett.*, *29*(17), 1836, doi:10.1029/2002GL015357.
Holben, B. N., et al. (1998), AERONET—A federated instrument network and data archive for aerosol characterization, *Remote Sens. Environ.*, *66*, 1–16.
Holben, B. N., et al. (2001), An emerging ground-based aerosol climatology: Aerosol optical depth from AERONET, *J. Geophys. Res.*, *106*, 12,067–12,097, doi:10.1029/2001JD900014.
Holben, B. N., T. F. Eck, I. Slutsker, A. Smirnov, A. Sinyuk, J. S. Schafer, D. Giles, and O. Dubovik (2006), AERONET's version 2.0 quality assurance criteria, *Soc. Photo-Opt. Instrum. Eng.*, *6408*, doi:10.1117/12.706524.
Intergovernmental Panel on Climate Change (2007), *Climate Change 2007: The Physical Science Basis. Contribution of Working Group I to the Fourth Assessment Report of the Intergovernmental Panel on Climate Change*, edited by S. Solomon et al., Cambridge Univ. Press, Cambridge, U. K.
Intergovernmental Panel on Climate Change (2013), *Climate Change 2013: The Physical Science Basis. Contribution of Working Group I to the Fifth Assessment Report of the Intergovernmental Panel on Climate Change*, edited by T. F. Stocker et al., Cambridge Univ. Press, Cambridge, U. K.
Jung, J., Y. J. Kim, K. Y. Lee, M. G. Cayetano, T. Batmunkh, J. H. Koo, and J. Kim (2010), Spectral optical properties of long-range transport Asian dust and pollution aerosols over Northeast Asia in 2007 and 2008, *Atmos. Chem. Phys.*, *10*, 5391–5408.
Karydis, V. A., A. P. Tsimpidi, W. Lei, L. T. Molina, and S. N. Pandis (2011), Formation of semivolatile inorganic aerosols in the Mexico City Metropolitan Area during the MILAGRO campaign, *Atmos. Chem. Phys.*, *11*, 13,305–13,323.
Khatri, P., T. Takamura, A. Shimizu, and N. Sugimoto (2014), Observation of low single scattering albedo of aerosols in the downwind of the East Asian desert and urban areas during the inflow of dust aerosols, *J. Geophys. Res. Atmos.*, *119*, 787–802, doi:10.1002/2013JD019961.
Kim, B. M., S. Teffera, and M. D. Zeldin (2000), Characterization of $PM_{2.5}$ and PM_{10} in the South Coast air basin of Southern California: Part 1—Spatial variations, *J. Air Waste Manage. Assoc.*, *50*(12), 2034–2044.
Kim, D., M. Chin, H. Yu, T. F. Eck, A. Sinyuk, A. Smirnov, and B. N. Holben (2011), Dust optical properties over North Africa and Arabian Peninsula derived from the AERONET dataset, *Atmos. Chem. Phys.*, *11*, 10,733–10,741.
Kim, J. (2008), Transport routes and source regions of Asian dust observed in Korea during the past 40 years (1965–2004), *Atmos. Environ.*, *42*, 4778–4789.
Kim, J., J. Lee, H. C. Lee, A. Higurashi, T. Takemura, and C. H. Song (2007), Consistency of the aerosol type classification from satellite remote sensing during the Atmospheric Brown Cloud–East Asia Regional Experiment campaign, *J. Geophys. Res.*, *112*, D22S33, doi:10.1029/2006JD008201.
Kim, S.-W., S.-C. Yoon, A. Jefferson, J. A. Ogren, E. G. Dutton, J.-G. Won, Y. S. Ghim, B.-I. Lee, and J.-S. Han (2005), Aerosol optical, chemical and physical properties at Gosan, Korea during Asian dust and pollution episodes in 2001, *Atmos. Environ.*, *39*, 39–50.
Kim, S.-W., S.-C. Yoon, J. Kim, and S.-Y. Kim (2007), Seasonal and monthly variations of columnar aerosol optical properties over east Asia determined from multi-year MODIS, LIDAR, and AERONET Sun/sky radiometer measurements, *Atmos. Environ.*, *41*, 1634–1651.
Kim, S.-W., S.-C. Yoon, and J. Kim (2008), Columnar Asian dust particle properties observed by Sun/sky radiometers from 2000 to 2006 in Korea, *Atmos. Environ.*, *42*, 492–504.
Kirchstetter, T. W., T. Novakov, and P. V. Hobbs (2004), Evidence that the spectral dependence of light absorption by aerosols is affected by organic carbon, *J. Geophys. Res.*, *109*, D21208, doi:10.1029/2004JD004999.
Lack, D. A., and C. D. Cappa (2010), Impact of brown and clear carbon on light absorption enhancement, single scatter albedo and absorption wavelength dependence of black carbon, *Atmos. Chem. Phys.*, *10*, 4207–4220, doi:10.5194/acp-10-4207-2010.
Lee, J., J. Kim, C. H. Song, S. B. Kim, Y. Chun, B. J. Sohn, and B. N. Holben (2010), Characteristics of aerosol types from AERONET sunphotometer measurements, *Atmos. Environ.*, *44*, 3110–3117.
Lee, S., S.-C. Yoon, S.-W. Kim, Y. P. Kim, Y. S. Ghim, J.-H. Kim, C.-H. Kang, Y. J. Kim, L.-S. Chang, and S.-J. Lee (2012), Spectral dependency of light scattering/absorption and hygroscopicity of pollution and dust aerosols in Northeast Asia, *Atmos. Environ.*, *50*, 246–254.
Levine, J. S., W. R. Cofer, D. R. Cahoon, and E. L. Winstead (1995), A driver for global change, *Environ. Sci. Technol.*, *29*, 120A–125A, doi:10.1021/es00003a746.
Levy, R. C., L. A. Remer, and O. Dubovik (2007), Global aerosol optical properties and application to Moderate Resolution Imaging Spectroradiometer aerosol retrieval over land, *J. Geophys. Res.*, *112*, D13210, doi:10.1029/2006JD007815.
Lim, H.-J., and B. J. Turpin (2002), Origins of primary and secondary organic aerosol in Atlanta: Results of time-resolved measurements during the Atlanta supersite experiment, *Environ. Sci. Technol.*, *36*, 4489–4496, doi:10.1021/es0206487.
Lim, S., M. Lee, G. Lee, S. Kim, S. Yoon, and K. Kang (2012), Ionic and carbonaceous compositions of PM_{10}, $PM_{2.5}$ and $PM_{1.0}$ at Gosan ABC Superstation and their ratios as source signature, *Atmos. Chem. Phys.*, *12*, 2007–2024.
Liu, D., J. Allan, D. Young, H. Coe, D. Beddows, Z. Fleming, M. Flynn, M. Gallagher, R. Harrison, and J. Lee (2014), Size distribution, mixing state and source apportionment of black carbon aerosol in London during wintertime, *Atmos. Chem. Phys.*, *14*, 10,061–10,084.
Mielonen, T., A. Arola, M. Komppula, J. Kukkonen, J. Koskinen, G. de Leeuw, and K. E. J. Lehtinen (2009), Comparison of CALIOP level 2 aerosol subtypes to aerosol types derived from AERONET inversion data, *Geophys. Res. Lett.*, *36*, L18804, doi:10.1029/2009GL039609.
Minoura, H., K. Takahashi, J. C. Chow, and J. G. Watson (2006), Multi-year trend in fine and coarse particle mass, carbon, and ions in downtown Tokyo, Japan, *Atmos. Environ.*, *40*(14), 2478–2487.
Omar, A. H., J.-G. Won, D. M. Winker, S.-C. Yoon, O. Dubovik, and M. P. McCormick (2005), Development of global aerosol models using cluster analysis of Aerosol Robotic Network (AERONET) measurements, *J. Geophys. Res.*, *110*, D10S14, doi:10.1029/2004JD004874.
Pathak, R. K., W. S. Wu, and T. Wang (2009), Summertime $PM_{2.5}$ ionic species in four major cities of China: Nitrate formation in an ammonia-deficient atmosphere, *Atmos. Chem. Phys.*, *9*(5), 1711–1722.

Pöschl, U. (2005), Atmospheric aerosols: Composition, transformation, climate and health effects, *Angew. Chem., Int. Ed.*, *44*(46), 7520–7540.
Prats, N., V. E. Cachorro, A. Berjón, C. Toledano, and A. M. De Frutos (2011), Column-integrated aerosol microphysical properties from AERONET Sun photometer over southwestern Spain, *Atmos. Chem. Phys.*, *11*, 12,535–12,547.
Putaud, J.-P., et al. (2004), A European aerosol phenomenology—2: Chemical characteristics of particulate matter at kerbside, urban, rural and background sites in Europe, *Atmos. Environ.*, *38*(16), 2579–2595.
Querol, X., et al. (2008), PM speciation and sources in Mexico during the MILAGRO-2006 Campaign, *Atmos. Chem. Phys.*, *8*, 111–128.
Quinn, P. K., and T. S. Bates (2005), Regional aerosol properties: Comparisons of boundary layer measurements from ACE 1, ACE 2, Aerosols99, INDOEX, ACE Asia, TARFOX, and NEAQS, *J. Geophys. Res.*, *110*, D14202, doi:10.1029/2004JD004755.
Reid, J. S., R. Koppmann, T. F. Eck, and D. P. Eleuterio (2005), A review of biomass burning emissions part II: Intensive physical properties of biomass burning particles, *Atmos. Chem. Phys.*, *5*, 799–825, doi:10.5194/acp-5-799-2005.
Russell, P. B., et al. (2002), Comparison of aerosol single scattering albedos derived by diverse techniques in two North Atlantic experiments, *J. Atmos. Sci.*, *59*, 609–619.
Russell, P. B., R. W. Bergstrom, Y. Shinozuka, A. D. Clarke, P. F. DeCarlo, J. L. Jimenez, J. M. Livingston, J. Redemann, O. Dubovik, and A. Strawa (2010), Absorption Angstrom Exponent in AERONET and related data as an indicator of aerosol composition, *Atmos. Chem. Phys.*, *10*, 1155–1169.
Russell, P. B., M. Kacenelenbogen, J. M. Livingston, O. P. Hasekamp, S. P. Burton, G. L. Schuster, M. S. Johnson, K. D. Knobelspiesse, J. Redemann, and S. Ramachandran (2014), A multiparameter aerosol classification method and its application to retrievals from spaceborne polarimetry, *J. Geophys. Res. Atmos.*, *119*, 9838–9863, doi:10.1002/2013JD021411.
Schafer, J. S., T. F. Eck, B. N. Holben, P. Artaxo, and A. F. Duarte (2008), Characterization of the optical properties of atmospheric aerosols in Amazônia from long-term AERONET monitoring (1993–1995 and 1999–2006), *J. Geophys. Res.*, *113*, D04204, doi:10.1029/2007JD009319.
Schuster, G. L., O. Dubovik, and B. N. Holben (2006), Angstrom exponent and bimodal aerosol size distribution, *J. Geophys. Res.*, *111*, D07207, doi:10.1029/2005JD006328.
Seinfeld, J. H., and S. N. Pandis (1998), *Atmospheric Chemistry and Physics: From Air Pollution to Climate Change*, John Wiley, New York.
Smirnov, A., B. N. Holben, T. F. Eck, O. Dubovik, and I. Slutsker (2000), Cloud-screening and quality control algorithms for the AERONET database, *Remote Sens. Environ.*, *73*, 337–349.
Smirnov, A., B. N. Holben, Y. J. Kaufman, O. Dubovik, T. F. Eck, I. Slutsker, C. Pietras, and R. N. Halthore (2002), Optical properties of atmospheric aerosol in maritime environments, *J. Atmos. Sci.*, *59*, 501–523.
Smirnov, A., et al. (2011), Maritime aerosol network as a component of AERONET—First results and comparison with global aerosol models and satellite retrievals, *Atmos. Meas. Tech.*, *4*, 583–597, doi:10.5194/amt-4-583-2011.
Sun, J., M. Zhang, and T. Liu (2001), Spatial and temporal characteristics of dust storms in China and its surrounding regions, 1960–1999: Relations to source area and climate, *J. Geophys. Res.*, *106*, 10,325–10,333, doi:10.1029/2000JD900665.
Takamura, T., T. Nakajima, and SKYNET Community Group (2004), Overview of SKYNET and its activities, *Opt. Pura Apl.*, *37*, 3303–3308.
Taylor, J., J. Allan, G. Allen, H. Coe, P. Williams, M. Flynn, M. Le Breton, J. Muller, C. Percival, and D. Oram (2014), Size-dependent wet removal of black carbon in Canadian biomass burning plumes, *Atmos. Chem. Phys.*, *14*, 13,755–13,771.
Tesche, M., A. Ansmann, D. Müller, D. Althausen, R. Engelmann, V. Freudenthaler, and S. Groß (2009), Vertically resolved separation of dust and smoke over Cape Verde using multiwavelength Raman and polarization lidars during Saharan Mineral Dust Experiment 2008, *J. Geophys. Res.*, *114*, D13202, doi:10.1029/2009JD011862.
van Beelen, A., G. Roelofs, O. Hasekamp, J. Henzing, and T. Röckmann (2014), Estimation of aerosol water and chemical composition from AERONET Sun–sky radiometer measurements at Cabauw, the Netherlands, *Atmos. Chem. Phys.*, *14*, 5969–5987.
Wang, R., et al. (2012), Global emission of black carbon from motor vehicles from 1960 to 2006, *Environ. Sci. Technol.*, *46*, 1278–1284, doi:10.1021/es2032218.
Wang, S., L. Fang, X. Gu, T. Yu, and J. Gao (2011), Comparison of aerosol optical properties from Beijing and Kanpur, *Atmos. Environ.*, *45*, 7406–7414, doi:10.1016/j.atmosenv.2011.06.055.
World Health Organization/United Nations Environment Programme (1992), *Urban Air Pollution in Megacities of the World*, Blackwell, Oxford, U. K.
Wu, Z. J., Y. F. Cheng, M. Hu, B. Wehner, N. Sugimoto, and A. Wiedensohler (2009), Dust events in Beijing, China (2004–2006): Comparison of ground-based measurements with columnar integrated observations, *Atmos. Chem. Phys.*, *9*, 6915–6932.
Yang, M., S. G. Howell, J. Zhuang, and B. J. Huebert (2009), Attribution of aerosol light absorption to black carbon, brown carbon, and dust in China—Interpretations of atmospheric measurements during EAST-AIRE, *Atmos. Chem. Phys.*, *9*, 2035–2050.
Yu, X., B. Zhu, and M. Zhang (2009), Seasonal variability of aerosol optical properties over Beijing, *Atmos. Environ.*, *43*, 4095–4101.